Chemistry and Biochemistry Faculty Works

Chemistry and Biochemistry

2017

The Stress Granule Transcriptome Reveals Principles of mRNA Accumulation in Stress Granules

Sarah F. Mitchell
Loyola Marymount University, sarah.mitchell@lmu.edu

Recommended Citation
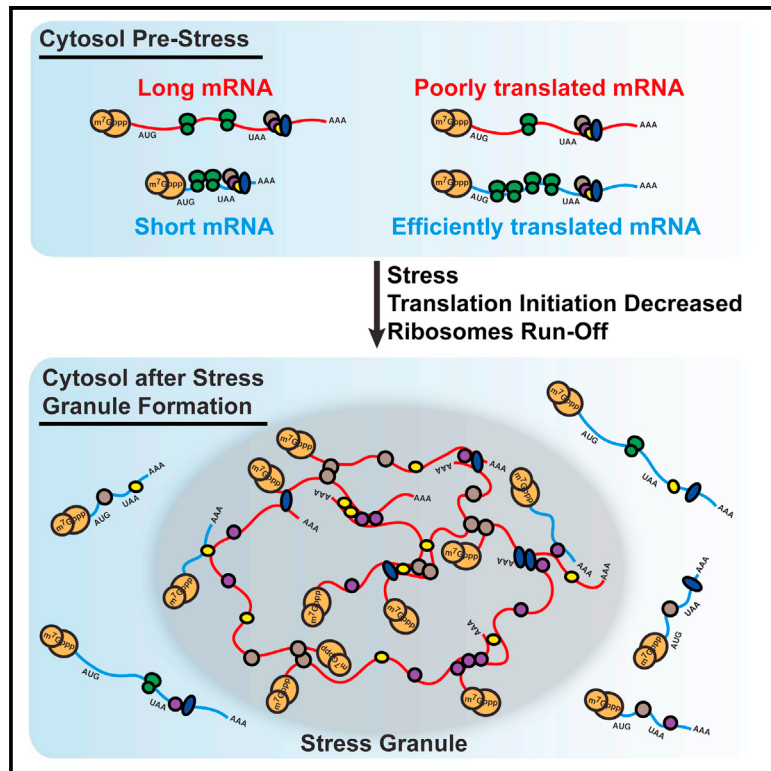
Khong, Anthony et. al. "The Stress Granule Transcriptome Reveals Principles of mRNA Accumulation in Stress Granules." Molecular Cell, vol. 68, no. 4, 11/2017, pp. 808-820.e5, doi:10.1016/j.molcel.2017.10.015.

The Stress Granule Transcriptome Reveals Principles of mRNA Accumulation in Stress Granules

Graphical Abstract

Authors

Anthony Khong, Tyler Matheny,
Saumya Jain, Sarah F. Mitchell,
Joshua R. Wheeler, Roy Parker

Correspondence

roy.parker@colorado.edu

In Brief

Transcriptome analysis coupled with single-molecule FISH validation of stress granule cores provides new insight into the mRNAs and ncRNAs that accumulate in stress granules. Ten percent of bulk mRNA molecules accumulate in stress granules, and targeting efficiency correlates with poorer translation efficiency and longer coding and UTR length.

Highlights

- Purification of stress granule cores identifies RNAs in stress granules

- Only ~10% of bulk mRNA molecules are present in stress granules

- Most mRNAs go to stress granules, but the efficiency varies from <1% to >95%

- Poor translation efficiency and longer length correlate with targeting to granules

CrossMark

CellPress

The Stress Granule Transcriptome Reveals Principles of mRNA Accumulation in Stress Granules

Anthony Khong,[1,2,5] Tyler Matheny,[2,5] Saumya Jain,[2,3] Sarah F. Mitchell,[2,4] Joshua R. Wheeler,[2] and Roy Parker[1,2,6,*]

[1]Howard Hughes Medical Institute, Chevy Chase, MD 20815, USA
[2]Department of Chemistry and Biochemistry, University of Colorado, Boulder, CO 80309, USA
[3]Present address: Department of Biological Chemistry, University of California, Los Angeles, CA 90024, USA
[4]Present address: Department of Chemistry and Biochemistry, Loyola Marymount University, Los Angeles, CA 90045, USA
[5]These authors contributed equally
[6]Lead Contact
*Correspondence: roy.parker@colorado.edu
https://doi.org/10.1016/j.molcel.2017.10.015

SUMMARY

Stress granules are mRNA-protein assemblies formed from nontranslating mRNAs. Stress granules are important in the stress response and may contribute to some degenerative diseases. Here, we describe the stress granule transcriptome of yeast and mammalian cells through RNA-sequencing (RNA-seq) analysis of purified stress granule cores and single-molecule fluorescence in situ hybridization (smFISH) validation. While essentially every mRNA, and some noncoding RNAs (ncRNAs), can be targeted to stress granules, the targeting efficiency varies from <1% to >95%. mRNA accumulation in stress granules correlates with longer coding and UTR regions and poor translatability. Quantifying the RNA-seq analysis by smFISH reveals that only 10% of bulk mRNA molecules accumulate in mammalian stress granules and that only 185 genes have more than 50% of their mRNA molecules in stress granules. These results suggest that stress granules may not represent a specific biological program of messenger ribonucleoprotein (mRNP) assembly, but instead form by condensation of nontranslating mRNPs in proportion to their length and lack of association with ribosomes.

INTRODUCTION

Stress granules (SGs) are non-membrane-bound assemblies of RNA and protein that form when translation initiation is limited (Protter and Parker, 2016; Buchan and Parker, 2009). SGs also share many protein components with neuronal granules, and mutations that increase SG formation or perturb SG clearance are implicated in degenerative diseases such as amyotrophic lateral sclerosis (ALS) and multisystem proteinopathy, where aberrant SG-like assemblies form (Buchan et al., 2013; Dewey et al., 2012; Kim et al., 2013b; Li et al., 2013; Mackenzie et al.,

2017; Ramaswami et al., 2013). SGs are thought to assemble via nontranslating mRNAs serving as scaffolds for RNA-binding proteins, which interact with each other through a variety of protein-protein interactions (Panas et al., 2016; Protter and Parker, 2016).

By super-resolution microscopy, SGs show denser regions of proteins and mRNAs (based on oligo(dT) fluorescence in situ hybridization [FISH]), referred to as cores, which can be biochemically purified (Jain et al., 2016). Cores are linked together by less concentrated regions of SG components referred to as a "shell," although whether the composition of the shell is different from cores has not been addressed (Jain et al., 2016). Purification of SG cores revealed the yeast and human SG core proteome is enriched in translation initiation factors, RNA-binding proteins, proteins with predicted prion-like domains (PrLDs), and proteins involved in neurodegenerative diseases (Jain et al., 2016). Intriguingly, SGs cores were also found to be composed of many proteins that were neither known to bind RNA nor predicted to contain PrLDs. Thus, this analysis identified many known classes of SG proteins while providing evidence for additional SG components.

Little is known about the RNA composition of SGs. SGs are known to contain non-translating mRNA from early reports showing that SGs contain PABP, stain positive for poly(A) mRNA, lack large ribosomal subunits, and are sensitive to drugs that alter the translation (Kedersha et al., 2000, 2002, 1999; McEwen et al., 2005). A few specific mRNAs have been shown to localize to SGs (Kedersha and Anderson, 2002; Nelles et al., 2016; Stoecklin et al., 2004; Stöhr et al., 2006), although the full population of mRNAs in SGs, and whether SGs contain specific noncoding RNAs (ncRNAs) or long intergenic noncoding RNAs (lincRNAs), has not been addressed.

Herein, we adapt our purification of SG cores to determine the transcriptome of both yeast and mammalian SG cores. We find that SGs are composed of over 80% mRNAs, although some lincRNAs and ncRNAs are enriched in SGs. SGs contain mRNAs from essentially every expressed gene, with no single mRNA or ncRNA representing more than 1% of the SG RNA molecules. Partitioning of specific mRNAs into SGs is decreased by efficient translation properties and increased by longer coding and UTR regions. By quantifying the composition of the SG transcriptome, we discover that only 10% of the bulk mRNA molecules

accumulate in SGs and that only 185 genes have more than 50% of their mRNA molecules present in SGs. These results suggest that SGs do not represent a specific biological program of messenger ribonucleoprotein (mRNP) assembly but instead form by condensation of untranslating mRNPs in proportion to their length and lack of association with ribosomes.

RESULTS

Mammalian SG Cores Are Enriched for Specific mRNAs

To determine the RNAs in mammalian SG cores, we purified and performed RNA sequencing (RNA-seq) in triplicate on SG cores isolated from U-2 OS cells after 60 min of arsenite exposure (Figure S1A; STAR Methods), referred to as $SG_{coreRNA}$. For each sample, 5% of the lysate was extracted for RNA-seq from the total RNA population, referred to as $total_{RNA}$. Pairwise correlation coefficients indicate reliable transcriptomes between $SG_{coreRNA}$ library triplicates and $total_{RNA}$ library triplicates (Figure S1B).

Pairwise correlation analysis between $SG_{coreRNA}$ and $total_{RNA}$ libraries demonstrate SG core transcriptomes are different from total RNA transcriptomes ($R^2 < 0.102$; Figure S1B). Supporting this analysis, out of the 15,689 transcripts identified (restricted to >1 fragments per kilobase of transcript per million mapped reads (FPKM) in $total_{RNA}$), 1,841 transcripts are enriched in SG cores (>2-fold change, $p < 0.01$), and 2,539 transcripts are depleted from SG cores (<0.5-fold change, $p < 0.01$) (Figure 1A; Table S1; Data S1). The remainder of the transcripts partitioned similarly between SG cores and the total RNA.

Validation of RNA-Seq by smFISH

To determine whether the $SG_{coreRNA}$ transcriptome was accurate, we examined several mRNAs that were, based on RNA-seq, preferentially enriched, neither enriched nor depleted, or preferentially depleted in SG cores by single-molecule fluorescence in situ hybridization (smFISH). We performed smFISH analysis on both stressed and unstressed U-2 OS cells for the following mRNAs: AHNAK (fold change [FC] is calculated as $FPKM_{SGcore}/FPKM_{total}$, FC = 6.92), DYNC1H1 (FC = 6.44), POLR2A (FC = 1.36), TFRC (FC = 1.10), PEG3 (FC = 5.69), CDK6 (FC = 3.35), ZNF704 (FC = 4.09), and GAPDH (FC = 0.29) (Figures 1B–1D and S1C).

The smFISH analyses revealed that AHNAK, DYNC1H1, PEG3, ZNF704, and CDK6 mRNAs are more enriched in SGs than POLR2A, TFRC, and GAPDH mRNAs (Figures 1B–1D and S1C), consistent with the RNA-seq results. By quantifying the number of transcripts in SGs and cells detected by smFISH, we observed that on average, 80% of AHNAK, 74% of PEG3, 70% of CDK6, 64% of ZNF704, and 53% of DYNC1H1 mRNAs are in SGs while 17%, 23%, and 4% of POLR2A, TFRC, and GAPDH mRNAs are in SGs, respectively (Figure 1E). These proportions parallel the enrichment of these mRNAs in SG cores by RNA-seq (Figure 1F). These numbers also reflect the SG core FPKM reads. For example, DYNC1H1 has roughly twice as many FPKM reads as POLR2A (183.8 and 80, respectively) and roughly twice as many average number transcripts in SG in cells as measured by smFISH (22 and 10, respectively) (Figure 1F). Therefore, the smFISH experiments indicate our transcriptome analysis of SG cores is valid.

The preferential recruitment of specific RNAs to SGs was examined with other SG markers, including PABP and Pumilio 2 (PUM2) (Figures S2A and S2B), indicating we are purifying RNAs enriched in bona fide SGs. Moreover, in ΔΔG3BP1/2 U-2 OS cells, which fail to form SGs under arsenite treatment (Kedersha et al., 2016), we no longer observe the clustering of SG-enriched mRNAs by smFISH (Figure S2B). These results argue we are identifying SG-enriched mRNAs.

Quantitative Analysis of the Bulk Transcriptome and SG Transcriptome

The combination of smFISH, which allowed us to count the number of specific mRNAs in the cell and within SGs, and RNA-seq data for the total and SG transcriptome allowed us to standardize our RNA-seq reads to the number of mRNAs per cell. We observed a linear relationship between individual mRNAs identified per cell by smFISH and FPKM values for each of these mRNAs (Figure 2A; $R^2 = 0.938$). Linear regression analysis allowed us to estimate the relative number of molecules of every mRNA in the cell based on its FPKM value (Table S1). We did not consider genes where the FPKM was less than 1, which allowed us to examine 11,195 mRNAs (STAR Methods). From this analysis, we estimate there are ~300,000 total mRNA molecules per cell, with mRNA abundance for different genes spanning from ~3,500 to <1 mRNA per cell. These numbers are in the same range as other estimates for mammalian cells (Schwanhäussser et al., 2011).

One possibility is that we are purifying only a subpopulation of mRNAs from SGs by isolating G3BP1 cores and that this is not an accurate representation of the complete RNA in SGs. To examine this, we looked at the relationship of the number of mRNA molecules in SGs for eight different mRNAs by smFISH and the FPKM values as determined by the SG core purification (Figure 2B). We excluded GAPDH mRNAs from this analysis because it is so abundant, we are unable to count all GAPDH mRNAs by smFISH reliably. We observed a linear relationship between the number of mRNAs within SGs identified by smFISH and the FPKM values from RNA-seq analysis of SG-core-purified RNA with good correlation (Figure 2B; $R^2 = 0.759$). At a minimum, this correlation of RNA-seq data with smFISH implies that the RNA composition of the shell is fairly similar to the core. More simply, we suggest that RNAs detected in the shell region by oligo(dT) FISH (Jain et al., 2016) are attached to, and co-purify with, cores once cells are lysed (see Discussion).

With this analysis, we can provide an approximation of the percent enrichment of every mRNA in SGs (Table S1; Data S1). It should be noted that these estimates are based on extrapolation from the transcripts we have examined by smFISH, and it remains possible that not all mRNAs will follow the same pattern. Nevertheless, we can estimate several features of the RNA content in SGs in 60-min arsenite stress. We estimate that there are roughly 42,000 RNA molecules in SGs, of which ~78% are mRNAs (Figures 2C and 2H). Only 0.6% of ncRNAs localize to SGs, while roughly 10% of mRNA molecules localize to SGs (Figures 2D and 2E). Consistent with this finding, we see a similar fraction of oligo(dT) staining (~13%) in SGs (Figures 2F and 2G), suggesting that our transcriptome analysis of SG cores captures most of the RNA content of SGs.
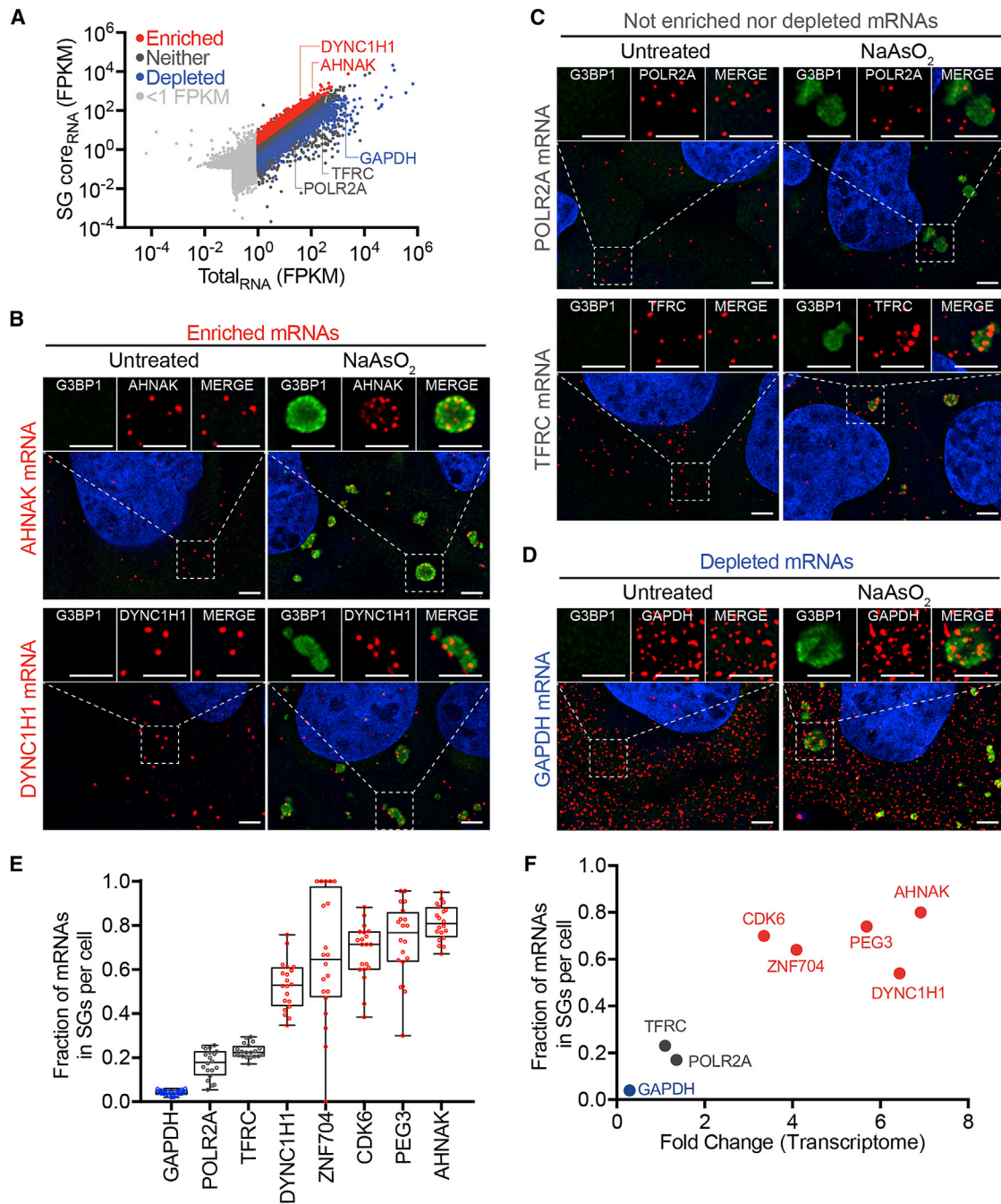
Figure 1. mRNAs Differ in Degree of Recruitment to SGs

(A) Scatterplot depicting RNA abundance (FPKM) in SG-purified RNA versus total RNA. Red dots indicate RNAs that are significantly enriched (fold change >2 and p < 0.01) in SG-purified RNA compared to total RNA. Blue dots indicate RNAs that are significantly depleted (fold change <0.5 and p > 0.01) in SG-purified RNA compared to total$_{RNA}$. Dark gray dots indicate RNAs that are either not significantly enriched or fail to meet the fold change requirement. Light gray dots indicate mRNAs below <1 FPKM.

(B) smFISH validation of mRNAs enriched in SGs (AHNAK and DYNC1H1).

(C) smFISH validation of RNAs that are neither enriched nor depleted from SGs (POLR2A and TFRC).

(D) smFISH validation of a mRNA that is depleted from SGs (GAPDH). Scale bar, 2 μm.

(E) Quantification of the fraction of each indicated transcript in SGs per cell. 20 cells were counted.

(F) Scatterplot depicting fraction of each indicated transcript in SGs versus FPKM ratios of SG$_{coreRNA}$-seq to total$_{RNA}$-seq data (fold-change). Twenty cells were counted for each experiment.
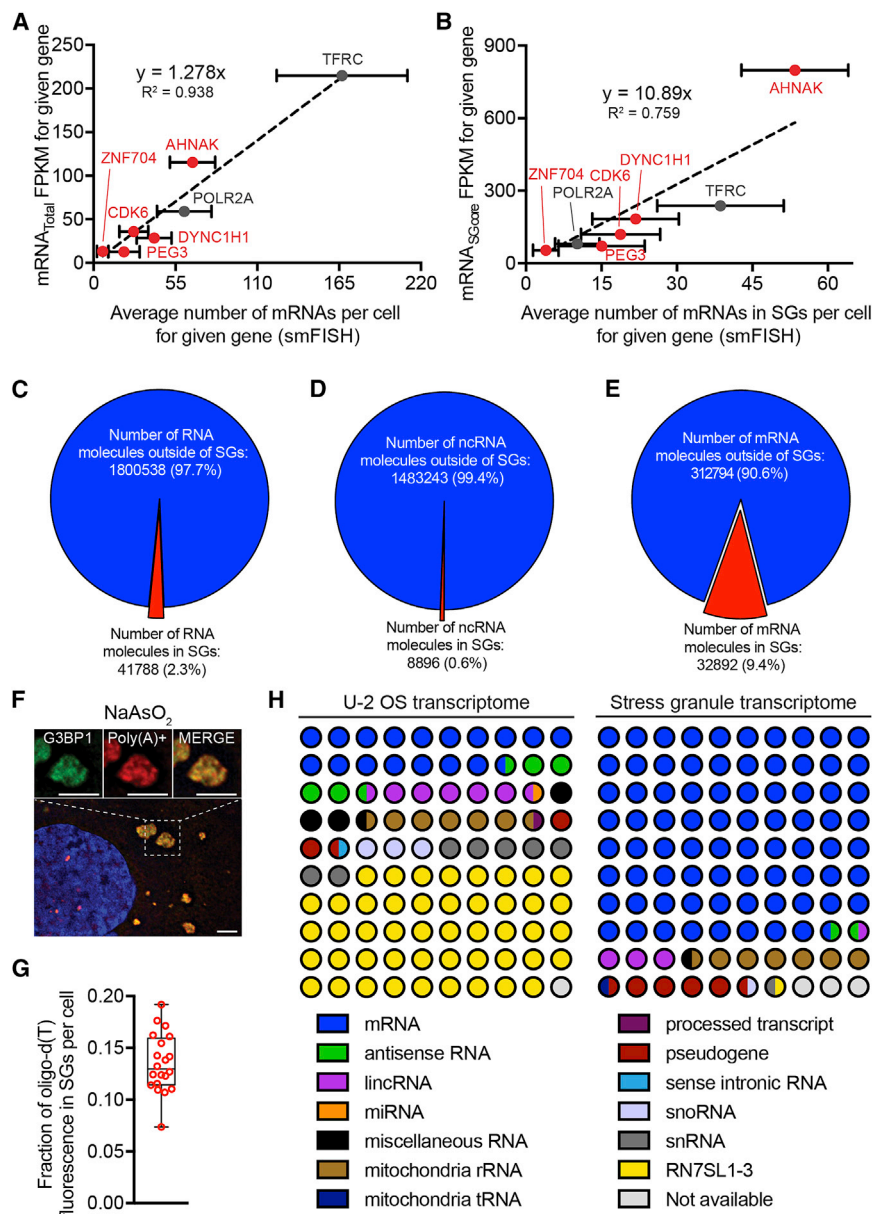
Figure 2. Quantitative Analysis of SG Composition

(A) Scatterplot depicting an average number of mRNAs per cell by smFISH versus FPKM values from total$_{RNA}$-seq data.

(B) Scatterplot depicting an average number of mRNAs in SGs per cell by smFISH versus FPKM values from SG$_{coreRNA}$-seq data. Error bars indicate 1 SD.

(C) Pie chart depicting the fraction of total RNA inside and outside SGs.

(D) Pie chart depicting the fraction of ncRNAs inside and outside SGs.

(E) Pie chart depicting the fraction of mRNAs inside and outside SGs.

(F) Oligo(dT) staining of sodium arsenite induced SGs. Scale bar, 2 μm.

(G) Quantitation of the fraction of oligo(dT) staining within SGs per cell.

(H) RNA composition of the U-2 OS transcriptome and the SGs transcriptome. RNA designations are from ensemble release 90.

stresses, and POLR2A mRNA is more highly enriched in SG during heat shock or sorbitol stress than during arsenite or thapsigargin stress. These results demonstrate that there are differences in the quantitative enrichment of specific mRNAs in SGs dependent on the stress condition, which could be due to differences in the specificity of translation repression during different stresses.

We also examined the localization of AHNAK and POLR2A mRNAs in U-2 OS ΔΔG3BP1/2 cells under heat shock. U-2 OS ΔΔG3BP1/2 cells cannot assemble SGs under arsenite and thapsigargin stress, but can assemble SGs under heat shock and sorbitol stress (Figure S2B) (Kedersha et al., 2016). We see enrichment of AHNAK mRNAs in heat shock-induced SGs in U-2 OS ΔΔG3BP1/2, but not POLR2A mRNAs (Figure S2B). This finding implies the RNA content of SGs is at least partially conserved in G3BP1/2-independent SGs.

mRNA Partitioning to SGs Is Largely Similar in Diverse Stresses

Since the protein components of SGs can vary under different stresses (Kedersha et al., 1999; Stoecklin et al., 2004), we examined whether the RNA composition varies under different stresses. We performed smFISH for several mRNAs (AHNAK, DYNC1H1, POLR2A, TFRC, and GAPDH) and quantified their enrichment in SGs in arsenite, thapsigargin, heat shock, or sorbitol-induced SGs (Kedersha et al., 2016; Kim et al., 2007).

We observed that there are similarities and differences between different stresses (Figures 3A–3D). For example, in all stresses, the GAPDH mRNA is depleted from SGs, while the AHNAK and DYNCH1 mRNAs are enriched. In contrast, TFRC is only enriched in SG during heat shock, with an ∼2-fold increase in the fraction of mRNAs in SGs compared to other

mRNAs Enriched in Mammalian SGs Have Less Ribosome Density

To determine how mRNAs are partitioned into SGs, we examined the properties of SG enriched, depleted, and evenly distributed mRNAs. We reasoned that translation efficiency might be a major determinant for localization during stress, because (1) decreased translation initiation induces SGs and (2) trapping ribosomes on transcripts with cycloheximide is sufficient to repress SG formation (reviewed in Panas et al., 2016; Protter and Parker, 2016). This rationale predicts that efficiently translated transcripts should be depleted from SGs, while inefficiently translated transcripts preferentially accumulate in SGs.
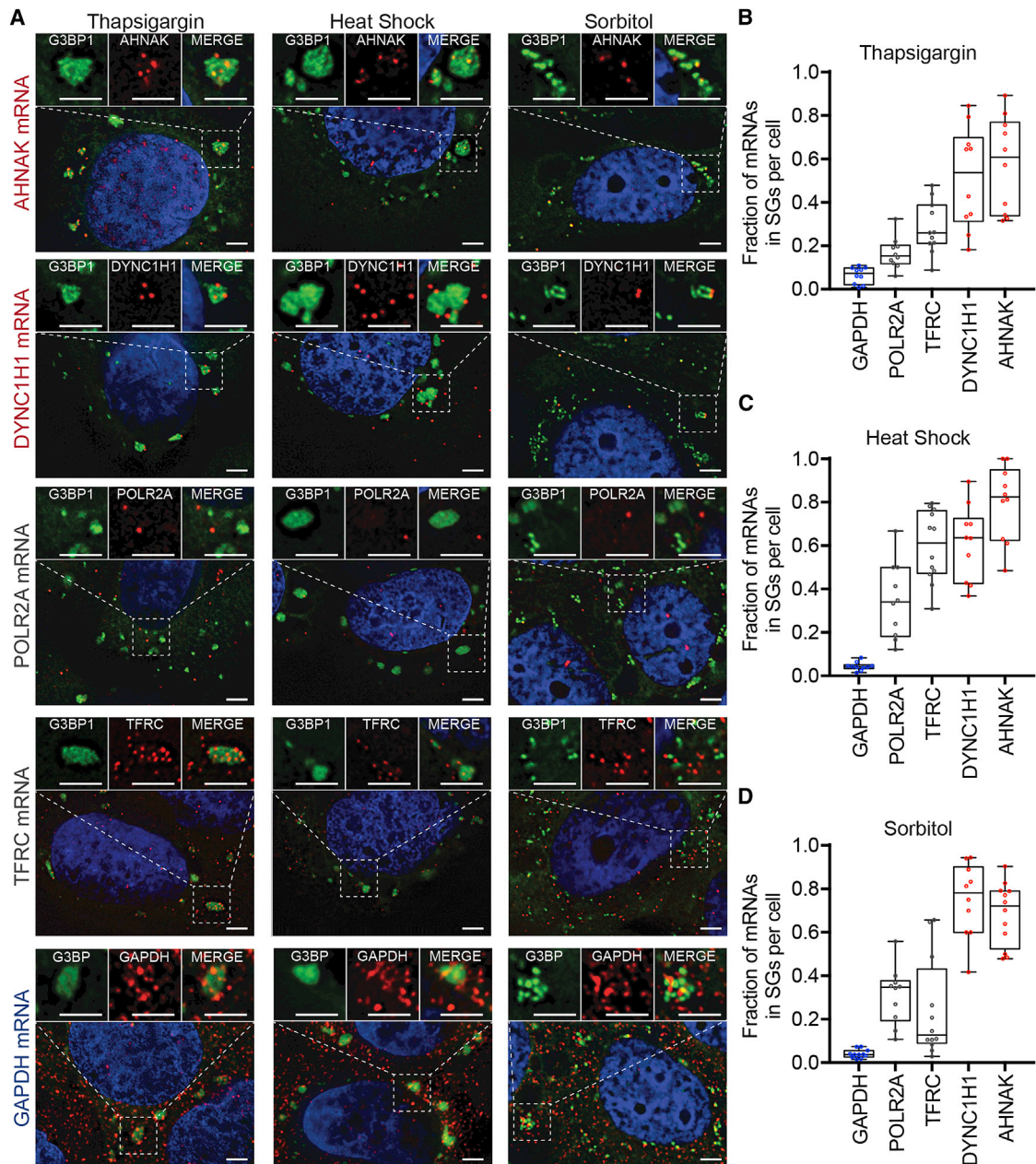
Figure 3. mRNA Localization Is Conserved during Multiple Stresses
(A) smFISH images acquired for five transcripts (AHNAK, DYNC1H1, TFRC, POLR2A, and GAPDH) during three different types of stresses (thapsigargin, heat shock, and sorbitol).
(B–D) Quantitation of each transcript's enrichment in SGs during (B) thapsigargin, (C) heat shock, and (D) sorbitol stress. Ten or more cells were counted for each experiment.

We compared our sequencing results to a previous report that examined translation efficiency (Sidrauski et al., 2015). For statistical purposes, we restrict our analysis for mRNA with FPKM in total RNA greater than 1 (approximately one transcript per cell) (Figure 2A). Out of this restricted list of 11,195 mRNAs, 14.5% were enriched in SGs (>2-fold change, p < 0.01) and 15.9% were depleted from SGs (<0.5 fold-change, p < 0.01) (Figures S3A and S3B). We found that transcripts with higher translation efficiency tend to be depleted from SGs, while transcripts with lower translation efficiency tend to localize to SGs (Figure 4A; STAR Methods). This finding demonstrates that one component that influences mRNA localization to SGs is the translation status of specific mRNAs. Since mRNAs that are poorly translated are generally less abundant and less stable (Radhakrishnan and Green, 2016), we also observed mRNAs enriched in SGs have a
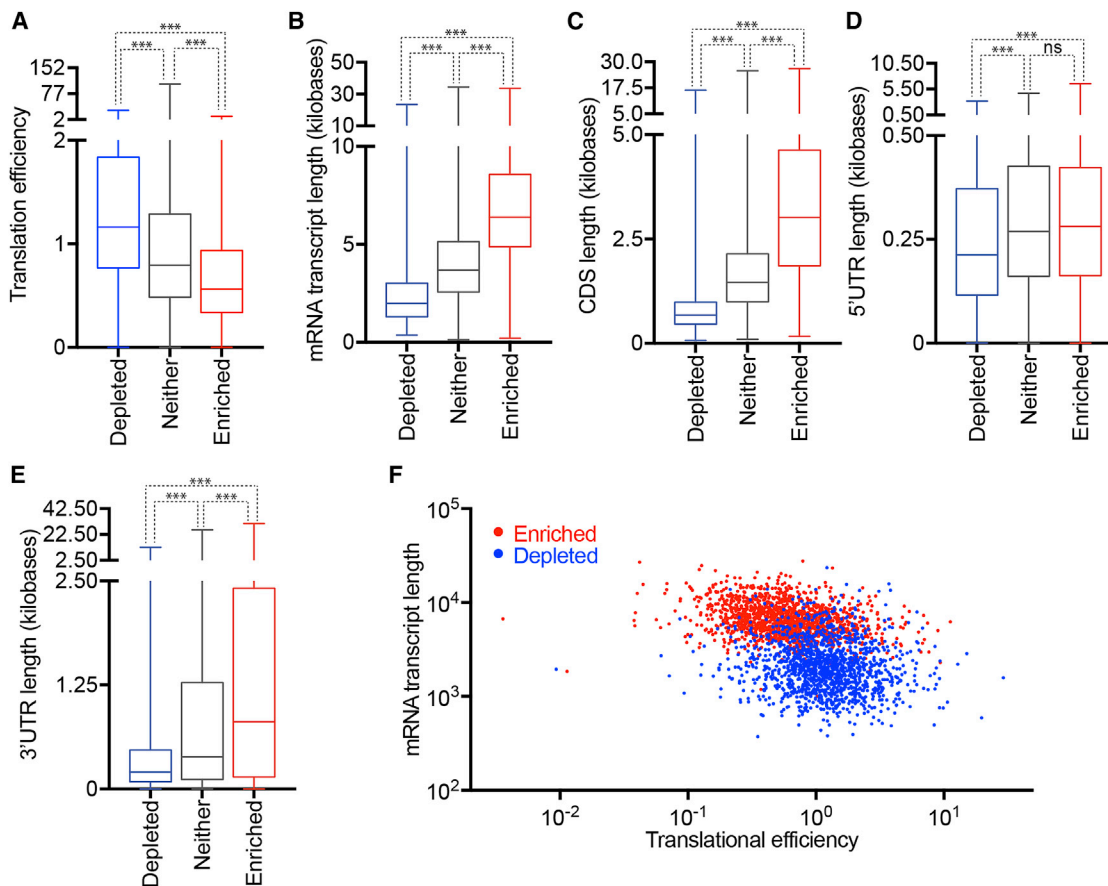
Figure 4. Physical Basis of Differential mRNA Recruitment to Mammalian SGs

(A–E) Boxplots depicting translational efficiency (A), total transcript length (B), coding sequence (CDS) length (C), 5′ UTR length (D), and 3′ UTR length (E) for each of the three classes of mRNA localization during stress: SG-enriched mRNAs, SG-depleted mRNAs, or neither.

(F) Scatterplot depicting the mRNA transcript length versus translational efficiency for SG-enriched (red) and SG-depleted (blue) mRNAs.

ns, not significant ($p > 0.05$); ***p value ≤ 0.001 (Student's t test).

shorter half life, are less abundant, and have less GC content (Figures S3C–S3E).

Mammalian SG-Enriched mRNAs Are Long

Examination of other metrics revealed SG-localized mRNAs were much longer (average length = 7.1 kb) than SG-depleted mRNAs (average length = 2.5 kb) and mRNAs that showed no preference for SGs (average length = 4.2 kb) (Figure 4B). Examination of the different contributions of the 5′ UTR, open reading frame (ORF), or 3′ UTR revealed that the length of the coding region showed the largest difference between enriched and depleted mRNAs in SGs, although the 3′ UTR also had an effect (Figures 4C–4E). We only observed slightly longer 5′ UTRs on SG-enriched mRNAs (Figure 4D), which could be because longer 5′ UTRs can decrease translation initiation due to RNA structure.

Given the overall dependence on mRNA length for accumulation in SGs, we also examined how the contributions of the 5′ and 3′ UTRs varied with the length of the coding region. The logic for this analysis was that for mRNAs with short coding regions, the 5′ UTR and 3′ UTR length might compensate for a shorter coding region. Therefore the 5′ and 3′ UTR effects might be more

obvious at shorter ORF lengths. Thus, we examined the contributions of the 5′ and 3′ UTR by first binning mRNAs by their ORF length and then determining whether there was a difference in the 5′ or 3′ UTR length for mRNAs accumulating in SGs compared to those depleted from SGs. We observed that 3′ UTR length made a significant difference for all coding regions size bins, but with a small effect once the mRNA coding region was over 3,000 bases (Figure S3F). A similar analysis for 5′ UTR length revealed the impact of longer 5′ UTR lengths was insignificant (Figure S3G). Taken together, these results indicate the length of the coding region and 3′ UTRs are important metrics for determining SG accumulation.

Mammalian SG-Enriched ncRNAs Are Long

We also examined the ncRNAs that are preferentially recruited to SGs. We restricted our analysis to ncRNA with FPKM in total RNA greater than 1. Out of these restricted 4,494 ncRNAs, 4.8% were enriched in SGs (>2-fold change, $p < 0.01$) and 16.9% were depleted from SGs (<0.5 fold-change, $p < 0.01$) (Figures 5A and 5B). Enriched ncRNAs (average length = 1.9 kb) tend to be longer than depleted ncRNA (average length = 0.9 kb) and
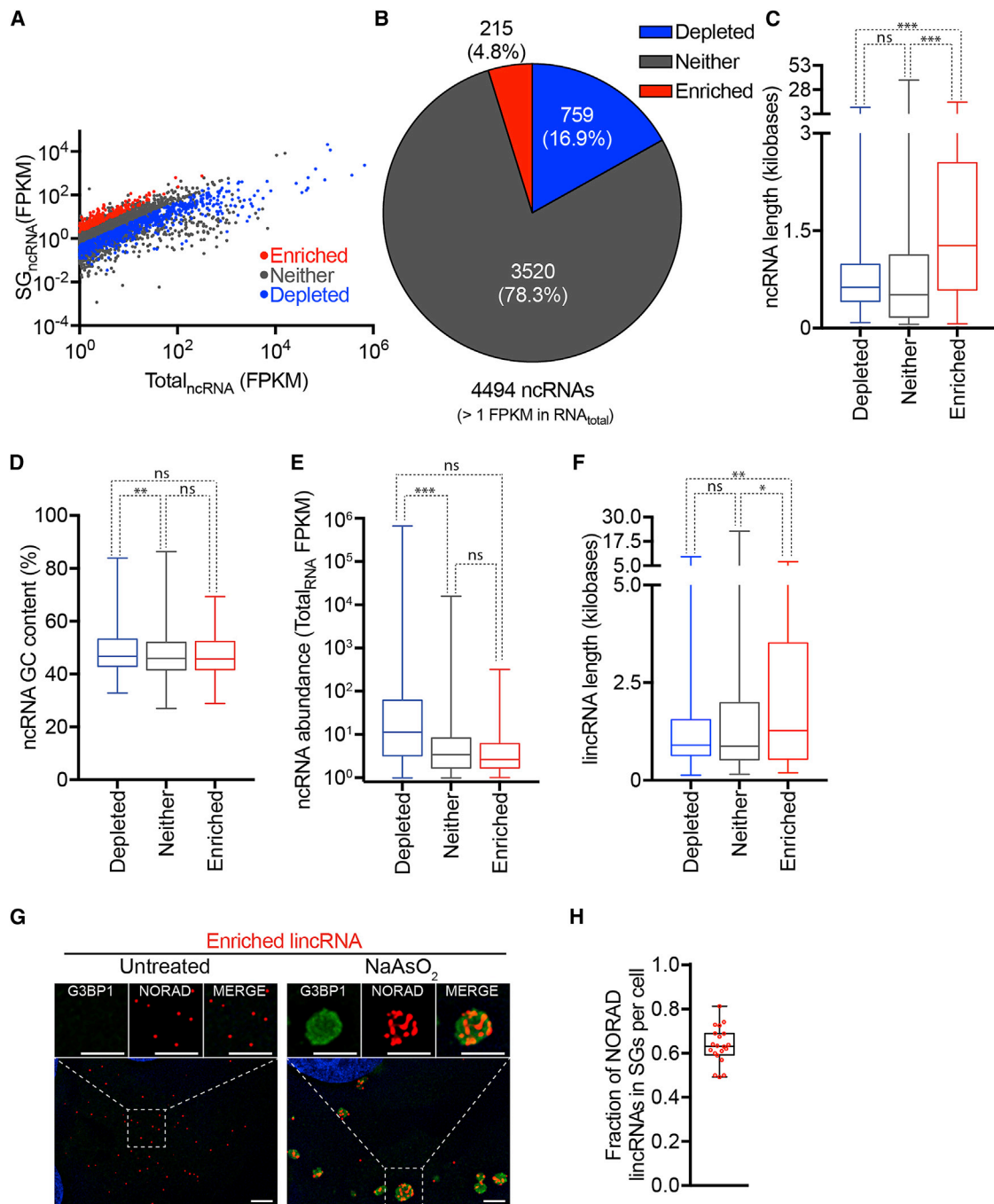
Figure 5. Physical Basis of Differential ncRNA Recruitment to Mammalian SGs

(A) Scatterplot depicting ncRNA abundance (FPKM) in SG-purified RNA versus total RNA. Red dots indicate ncRNAs that are significantly enriched (fold change >2 and p < 0.01) in SG-purified RNA compared to total RNA. Blue dots indicate ncRNAs that are significantly depleted (fold change <0.05 and p > 0.01) in SG-purified RNA compared to total RNA. Gray dots indicate ncRNAs that are either not significantly enriched or fail to meet the fold change requirement.

(B) Pie chart depicting the relative contribution of each class of ncRNA (SG enriched, SG depleted, or neither) to the total transcriptome SG transcriptome (right).

(C–F) Boxplot depicting the transcript length (C), GC content (D), abundance of ncRNA (E), and length of lincRNAs (F) for the three classes of localization: SG-enriched mRNAs, SG-depleted mRNAs, or neither. ns, p > 0.05; *p $\leq$ 0.05; **p $\leq$ 0.01; ***p $\leq$ 0.001 (Student's t test).

(G) smFISH images of an SG-enriched lincRNA, NORAD, during no stress and sodium arsenite-induced stress. Scale bar, 2 μm.

(H) Quantitation of the fraction of NORAD RNAs in SGs. Twenty cells were counted.

ncRNA that showed no preference for SGs (average length = 0.9 kb) (Figure 5C). GC content and abundance of ncRNA are not significant predictors of accumulation in SGs (Figures 5D and 5E).

Specific examination of lincRNAs revealed SG-enriched lincRNAs also tend to be longer (Figure 5F). We validated a lincRNA, non-coding RNA activated by DNA damage (NORAD), is enriched in SGs by smFISH (Figures 5G, 5H, and S2A). NORAD is one of the top 10 most enriched lincRNAs in SGs (Table S3A) and is thought to function as a Pumulio sponge (Lee et al., 2016; Tichon et al., 2016).

Length and Translation Efficiency Influence SG Targeting of RNAs in Yeast

To determine whether the principles of mRNA targeting to SGs observed in mammalian cells were conserved, we purified and sequenced the mRNAs within SG cores from *Saccharomyces cerevisiae* after induction of SGs by sodium azide for 30 min (Buchan et al., 2011). SG_{RNA} and $total_{RNA}$ were isolated from three independent biological replicates and sequenced. Reads from biological replicates of SG_{RNA} as well as $total_{RNA}$ were highly reproducible (Figure S4A).

Yeast RNA-seq reads from SG_{RNA} and $total_{RNA}$ showed little similarity to each other, indicating that a subset of cellular RNA is significantly enriched in SGs (Figures 6A and S4A; Table S2). By comparing reads across RNAs in SG_{RNA} and $total_{RNA}$, we found that 916 mRNAs were significantly (p value < 0.01) enriched in SG_{RNA} as compared to $total_{RNA}$, while 1,107 mRNAs were significantly enriched in $total_{RNA}$ as compared to SG_{RNA} (Figure 6A; Data S2). Thus, during stress in yeast, we observe the same three classes of mRNAs as in mammalian cells: one subset preferentially localized to SGs, another subset preferentially depleted from SGs, and a third subset partitioning similarly between SGs and the cytosol. smFISH for one SG-enriched mRNA, MDM1, validated that it accumulated in SGs (Figure S4B).

Multiple lines of evidence suggest that poorly translated mRNAs localize to yeast SGs, while efficiently translated mRNAs are depleted. First, we observed that predicted ribosome density and translation initiation rates for SG-depleted mRNAs are significantly higher than the predicted rates for SG-enriched mRNAs (p value < 0.0001; Figures 6B and S4C) (Siwiak and Zielenkiewicz, 2010). Second, we observe fraction of optimal codons per transcript, which is a metric for translation efficiency (Presnyak et al., 2016), strongly correlates with the distribution of mRNAs. Specifically, SG-enriched mRNAs have an average of 43.9% optimal codons, and SG-depleted mRNAs have an average of 59.6% optimal codons (p value < 0.0001; Figure 6C). Consistent with the observation that SG-enriched mRNAs are composed of non-optimal codons, and the observation that non-optimal codons decrease a transcript's stability (Presnyak et al., 2016), we also found that SG-enriched mRNAs are less stable than SG-depleted mRNAs (Figure S4D).

Similar to mammalian cells, we found that the average SG-enriched mRNA length in yeast (2.7 kb) is significantly longer than SG-depleted mRNAs (1.1 kb) (Figure 6D) (Nagalakshmi et al., 2008). This length dependence in yeast is driven primarily by ORF length and not by 5′ UTR or 3′ UTR length, which is consistent with the overall shorter 3′ UTR length in yeast (Figures 6F–6H).

Thus, similar to mammalian cells, the major metrics for mRNA accumulation in yeast SGs are length and poor translation efficiency (Figures 4F and 6E). Indeed, mathematical models made by machine learning and based solely on length and codon optimality (or ribosome density for mammalian mRNAs) are sufficient to accurately predict whether a mRNA will be enriched or depleted from SGs for 75.9% of the yeast mRNAs and 74.1% of mammalian mRNAs (Figure S5; STAR Methods).

Yeast SGs Contain Non-coding RNAs

Since we observed that mammalian SGs contain ncRNAs, we wanted to examine whether yeast SGs contain ncRNA as well. In yeast, we identified some stable untranslated transcripts (SUTs) (Xu et al., 2009) that accumulate in SGs (Figure S4E; Data S3). The SUTs enriched in SGs were significantly longer than SG-depleted SUTs (Figure S4G). In addition, cryptic unstable transcripts (CUTs), which are a class of non-coding RNAs that are related to SUTs (Xu et al., 2009) but much shorter (200–800 nt), are rarely enriched in SGs (Figure S4F). Again, SG-enriched CUTs were longer than SG-depleted CUTs (Figure S4H). The inclusion of ncRNAs in SGs demonstrates that prior translation per se is not a requisite for RNA accumulation in SGs and that length plays a role in targeting both coding and noncoding transcripts to SGs.

Membrane Association Limits SG Partitioning of mRNA

Analysis of the SG transcriptome reveals that mRNAs associated with membranes are depleted from SGs, which was suggested by early observations that mRNAs localizing to the ER do not localize to SGs (Unsworth et al., 2010). Specifically, by comparison of the yeast-SG-enriched mRNAs to mRNAs associated with the endoplasmic reticulum (ER) through signal recognition particle (SRP) interactions (Chartron et al., 2016), we found that SG-enriched mRNAs are significantly distinct from the subset of mRNAs encoding proteins that localized via SRP (Figure S6A), while SG-depleted mRNAs showed significant overlap with ER-localized mRNAs. Consistent with this observation, we find that human-SG-enriched mRNAs are significantly distinct from the subset of mRNAs encoding proteins that are secreted (Figure S6C) (Uhlen et al., 2010; Uhlén et al., 2015). We also found that SG-enriched mRNAs in both yeast and mammalian cells were significantly distinct from mRNAs that encode proteins that localize to the mitochondria (Figures S6B and S6D) (Chartron et al., 2016) (Calvo et al., 2015; Pagliarini et al., 2008), while SG-depleted mRNAs showed significant overlap with mRNAs encoding mitochondria-localized proteins (Figures S6B and S6D).

Taken together, these findings suggest that mRNA localization to other organelles may preclude mRNA from efficiently partitioning into SGs, which could be explained by restricted diffusion when mRNAs are bound to membrane surfaces. It should be noted that we cannot rule out the formal possibility that a subset of SGs form on the ER or mitochondrial surface and such membrane-associated SGs do not purify efficiently in our biochemical preparations.

SG-Enriched mRNAs Are Modestly Enriched for SG-Resident Proteins

One model for mRNA recruitment to SGs is that SG-enriched mRNAs would bind more SG-targeted RNA-binding proteins, and the accumulation of those proteins in SGs would then
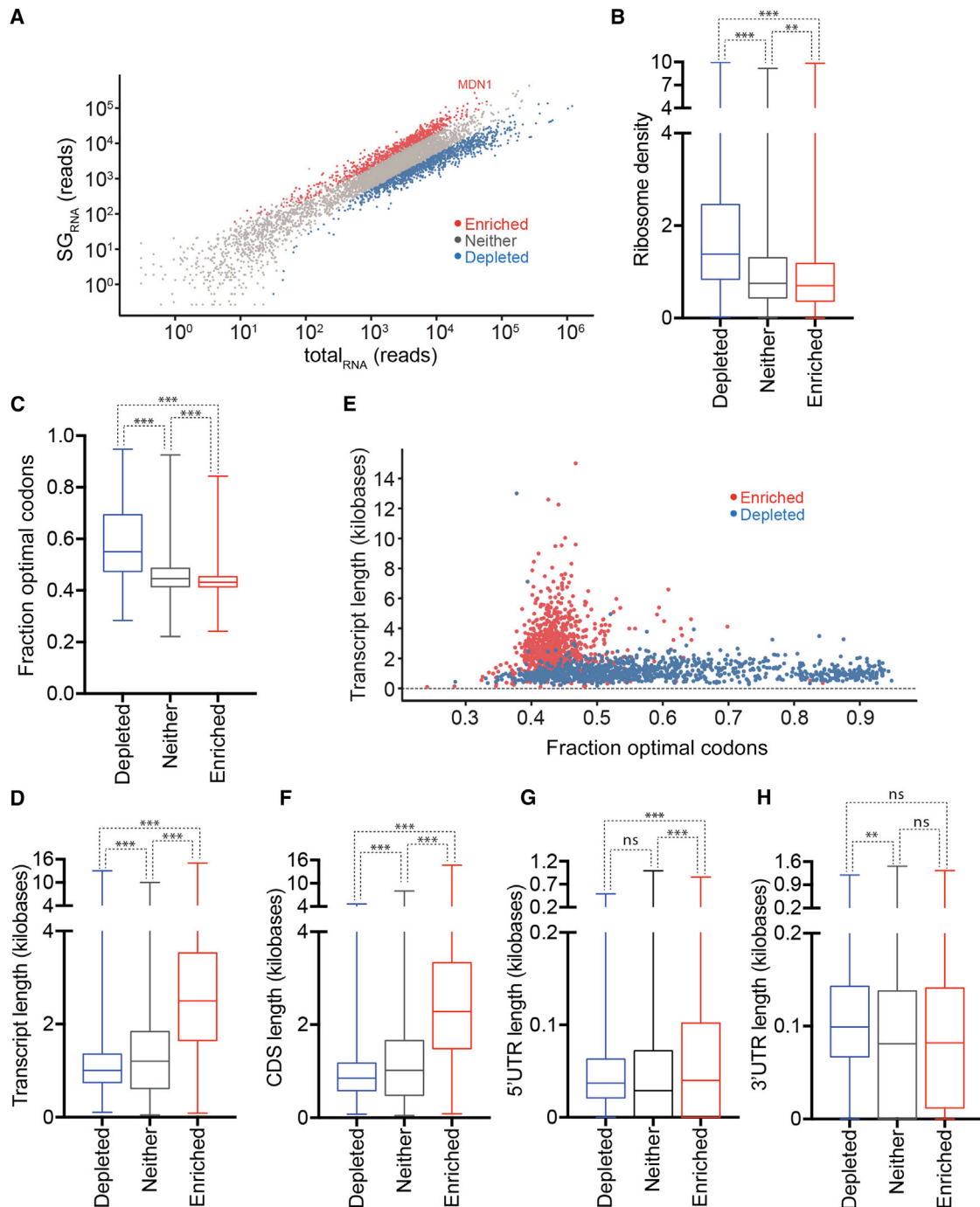
Figure 6. The Physical Basis of mRNA Localization to SGs Is Conserved from Mammals to Yeast

(A) Scatterplot depicting normalized RNA-seq reads from libraries made from yeast-SG-purified RNA versus total RNA.

(B and C) Boxplots depicting two metrics of translatability, ribosome density (B) and codon optimality (C), are correlated with altered localization during stress.

(D) Boxplot depicting how transcript length correlates with altered localization.

(E) Scatterplot of transcript length versus fraction optimal codons for SG-enriched (red) and SG-depleted mRNAs (blue).

(F–H) Boxplots depicting how length correlates with localization for the CDS (F), the 5′ UTR (G), and the 3′ UTR (H).

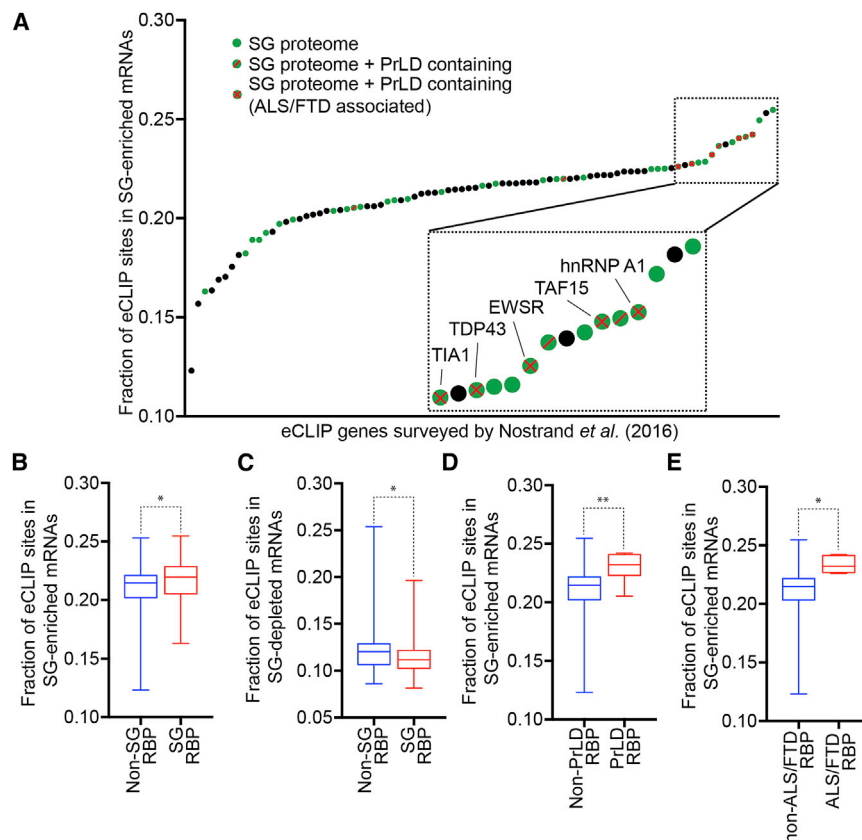ns, $p > 0.05$; **$p \leq 0.01$; ***$p \leq 0.001$ (Student's t test).

Figure 7. SG-Enriched mRNAs Are Enriched for SG-Resident Proteins

(A) Survey of RNA-binding proteins from Van Nostrand et al. (2016) plotted against the fraction of eCLIP sites found in SG-enriched mRNAs. Green dots are SG-resident RBPs. Black dots are non-SG-resident RBPs. Green dots with a red diagonal line are SG-resident RBPs with a PrLD domain. Green dots with a red X are SG-resident RBPs with a PrLD domain and are associated with ALS/FTD.

(B and C) Boxplot illustrating the fraction of eCLIP sites found in SG-enriched mRNAs (B) or SG-depleted mRNAs (C) from SG-resident RBPs or non-SG RBPs. Boxplot depicting the fraction of eCLIP sites found in SG-depleted mRNAs from SG-RBPs or non-SG RBPs.

(D and E) Boxplot illustrating the fraction of eCLIP sites found in SG-enriched RNAs from SG RBPs containing PrLD (D) and RBPs associated with ALS/FTD (E). *p $\leq$ 0.05; **p $\leq$ 0.01 (Student's t test).

may both enhance the formation of aberrant pathological aggregates and contribute to disease progression (Li et al., 2013; Ramaswami et al., 2013).

DISCUSSION

Based on determining the SG transcriptome in yeast and mammalian cells, we demonstrate several principles of RNA accumulation in SGs. One key observation is that SGs are primarily accumulations of diverse mRNAs. For example, analyses in mammalian cells showed SG are >78% mRNAs, although some ncRNAs can accumulate within SGs (Figures 2 and 5). Similarly, in yeast, RNA-seq genes indicates ~95% of the molecules in SGs are mRNAs. More strikingly, there is no overly abundant RNA within SGs, with the most abundant mRNAs in mammalian SGs, actin, only representing ~0.5% of the SG mRNAs (Figure 2E; Table S1B). Thus, SGs are a true composite of many mRNAs, which is also supported by the fact that essentially every mRNA is present in SGs to some extent. This is not an artifact of contaminating abundant RNA molecules, since smFISH for GAPDH, an abundant mRNA depleted from SGs, affirms that 4% of the GAPDH mRNA molecules are present within SGs (Figure 1). The fact that essentially every mRNA can accumulate in SGs suggests that the interactions required for SG accumulation are generic and are not limited to a specific subset of mRNAs.

Two key observations argue that we are effectively identifying the majority of RNAs within SGs. The first observation that we effectively identify the full spectrum of SG RNAs is that smFISH analysis of individual mRNAs, which identifies mRNAs anywhere within SGs, and RNA-seq analysis, which by definition is only sequencing RNAs present in the core region, show a strong linear correlation (Figure 2B). The second key observation is that based on the quantification of the RNA-seq of SG cores, we calculate that ~9.4% of the total mRNAs in the cell

partition specific mRNAs into SGs. A prediction of this model is that SG-enriched RNAs would be enriched for RNA-binding sites of known SG-localized ribonucleoproteins (RNPs). To test this prediction, we mined previously published enhanced cross-linking immunoprecipitation (eCLIP) datasets on both SG-resident (n = 36) and non-SG-resident (n = 51) RNPs by scoring eCLIP binding sites in SG-enriched RNAs (Figure 7A; Data S4) (Van Nostrand et al., 2016). We observed that RNA-binding proteins had, on average, ~22% of their eCLIP sites in mRNAs enriched in SG.

Surprisingly, we observed SG-localized RNA-binding proteins were only modestly enriched on SG-enriched mRNAs as compared to non-SG-resident RNA-binding proteins (Figure 7B; p = 0.0484). Similarly, SG-localized RNA-binding proteins were slightly underrepresented in SG-depleted mRNAs as compared to non-SG-resident RNA-binding proteins (Figure 7C; p value = 0.0486). Future experiments will be required to determine whether this modest enrichment is because these SG-resident RNA-binding proteins play a role in targeting mRNAs into SGs or whether they are identified as SG components because they show a slight preference for mRNAs that accumulate in SGs.

We also observed that RNA-binding proteins found in SGs with PrLDs, or those associated with degenerative diseases such as ALS or frontotemporal degeneration (FTD), showed an even greater bias to bind to mRNAs enriched in SGs (Figures 7A, 7D, and 7E). The enrichment of PrLD-containing proteins involved in disease with SG mRNAs is consistent with a model whereby the prevalent recruitment of these proteins into SGs

accumulate in SGs, which is similar to the 13% of total oligo(dT) staining that resides in SGs under the same conditions (Figures 2F and 2G). Thus, while it is possible we are selectively losing a subset of RNAs loosely associated with SGs, these two observations suggest we are efficiently identifying the vast majority of mRNAs associated with SGs. One simple explanation is that the staining of both proteins and RNAs in the shell region of SGs (Jain et al., 2016) is due to mRNAs of sufficient length that they have portions residing within the core region and thus co-purify with cores after cell lysate. However, two caveats should be noted. First, since we are purifying SG cores using G3BP1 as an affinity ligand, it is possible we are missing some mRNAs in SG, particularly if they accumulate in SG cores that are lacking in G3BP. Second, we may be underestimating the fraction of some RNAs in SGs if specific mRNAs in the shell region are lost during the purification process.

Two observations led to the striking conclusion that only 10%–12% of the total mRNA molecules in U-2 OS cells accumulate in SGs. First, 13% of the poly(A)$^+$ RNA signal accumulates in SG based on oligo(dT) FISH (Figures 2F and 2G). Second, by quantifying the distribution of the mRNA population, we calculated that ∼9%–10% of the mRNA molecules in the cell assemble into SGs (Figure 2E). Moreover, based on our standardization of the RNA-seq data by smFISH analysis (Figures 2A and 2B), we estimate that there are only 185 genes in which greater than 50% of the mRNA molecules are present in SGs. Thus, only a minority of the bulk mRNA population enters SGs, and only for <2% of the analyzed genes are the majority of the transcripts within SGs.

The diversity and overall minor amount of mRNA within SGs force us to reconsider their nature and possible function. First, the small amount of mRNA within SGs suggests that these structures will not have large global effects on bulk mRNA. This is consistent with observations that cell lines lacking G3BP, which fail to form SG, still efficiently repress global translation of mRNAs (Kedersha et al., 2016), and cells with defective SG formation do not show altered mRNA degradation (Bley et al., 2015). Thus, if SGs directly affect the function of mRNAs within them, SG formation will only have a substantial impact on the few mRNAs with a high percentage of their total molecules present in SGs. It remains possible that sequestering ∼10%–13% of the mRNAs in the cell has other impacts on cell physiology, such as affecting signaling pathways (Kedersha et al., 2013).

The transcriptome of SGs argues that every SG will be different in composition. Since total SG volume in U-2 OS cells is 10 μm^3, and each core is ∼0.0066 μm^3 (based on the size of cores using nanoparticle tracking; Jain et al., 2016), we estimate that there are between 300 and 1,500 SG cores in U-2 OS cells after 60 min of arsenite stress if SGs consist of 20% (estimated in Jain et al., 2016) or 100% (a maximal boundary condition) cores, respectively. Since actin mRNA, the most abundant molecule in SGs, has only 160 molecules within SGs per cell and there are at least 300 cores per cell by our most conservative estimate, the RNA composition of SG cores must be heterogeneous. Moreover, at 1 hr of arsenite stress, we estimate there are 32,000 mRNAs in SGs (Figure 2E). Thus, each core should have ∼21 to 106 mRNA molecules, and by necessity, cores

would need to be composed of a heterogeneous mixture of transcripts to explain our transcriptome data.

We identify three parameters that correlate with the partitioning of specific mRNAs into SGs. First, both yeast and mammalian analyses show inefficient translation correlates with higher partitioning of mRNAs into SGs (Figures 4 and 5). This is consistent with prior models that mRNAs engaged with ribosomes are restricted from entering SGs and provides additional evidence that mRNAs need to be nontranslating to accumulate within SG (Kedersha et al., 2000) (Kedersha and Anderson, 2002). Second, association with ER or mitochondrial membranes correlates with mRNAs being excluded from SGs, perhaps due to membrane tethering limiting the mRNPs from diffusing into SGs (Figure S6). Third, a strong and predominant metric of mRNA accumulation in SGs is the overall length of the coding region and the 3′ UTR in both yeast and mammalian SG transcriptomes and in both organisms is strongly linked to the length of the ORF (Figures 4 and 6).

In principle, a longer mRNA could be more efficiently localized to SGs by two potentially overlapping mechanisms. First, a longer coding region could increase SG partitioning by providing multiple binding sites for RNA-binding proteins that may target mRNAs into SGs. Although it has been tacitly assumed that mRNAs would enter SGs through the interactions of specific RNA-binding proteins, to our knowledge, there is no direct evidence in support of this model. Indeed, although actin mRNA has been localized to SGs, its association with SGs is independent of the ZBP1 RNA-binding protein (Stöhr et al., 2006). Moreover, we observe only a very modest bias in the binding of SG RNA-binding proteins to mRNAs enriched in SGs (Figure 7B). Thus, while mRNA-binding proteins can clearly play a role in the overall assembly of SGs (Panas et al., 2016; Protter and Parker, 2016), whether they dictate the specific mRNAs localized to SGs remains to be determined. An alternative model to long ORFs simply providing more RNA-binding protein (RBP) sites is that the condensation of mRNAs into SGs would be promoted by RNA-RNA interactions between the exposed coding regions and any 3′ UTR regions exposed due to the off-rate of mRNA-binding proteins and their redistribution into exposed coding regions. In this model, longer coding regions and/or the 3′ UTRs could allow for more RNA-RNA interactions. Thus, a key area of future research will be in determining what interactions define the SG transcriptome and how this affects mRNA function.

STAR★METHODS

Detailed methods are provided in the online version of this paper and include the following:

- KEY RESOURCES TABLE
- U-2 OS GROWTH CONDITIONS AND REAGENTS
- ISOLATION OF RNA FROM U-2 OS CELLS AND SG CORES FOR RNA-SEQUENCING
- MAMMALIAN LIBRARY CONSTRUCTION AND RNA-SEQUENCING
- ISOLATION AND SEQUENCING OF RNA FROM STRESS GRANULES
- YEAST LIBRARY CONSTRUCTION

- YEAST SEQUENCING DATA ANALYSIS
- YEAST LENGTH, TRANSLATION, AND STABILITY ANALYSIS
- MAMMALIAN SEQUENCING DATA ANALYSIS
- HUMAN LENGTH, TRANSLATION, AND STABILITY ANALYSIS
- eCLIP DATA ANALYSIS
- MACHINE LEARNING
- STATISTICAL TESTS
- STRESS CONDITIONS
- SEQUENTIAL IMMUNOFLUORESCENCE AND SINGLE MOLECULE FISH
- MICROSCOPY AND IMAGE ANALYSIS
- DATA AND SOFTWARE AVAILABILITY

SUPPLEMENTAL INFORMATION

Supplemental Information includes six figures, three tables, and five datasets and can be found with this article online at https://doi.org/10.1016/j.molcel.2017.10.015.

AUTHOR CONTRIBUTIONS

A.K., T.M., S.J., J.R.W., and S.F.M. conceived and performed experiments, analyzed results, and contributed to manuscript preparation. R.P. contributed to project conception and manuscript preparation.

REFERENCES

Aken, B.L., Ayling, S., Barrell, D., Clarke, L., Curwen, V., Fairley, S., Banet, J.F., Hourlier, T., Billis, K., Garc, C., et al. (2016). The Ensembl gene annotation system. Database 2016, 1–19.

Anders, S., and Huber, W. (2010). Differential expression analysis for sequence count data. Genome Biol. 11, R106.

Anders, S., Pyl, P.T., and Huber, W. (2015). HTSeq—a Python framework to work with high-throughput sequencing data. Bioinformatics 31, 166–169.

Bley, N., Lederer, M., Pfalz, B., Reinke, C., Fuchs, T., Glaß, M., Birgit, M., and Stefan, H. (2015). Stress granules are dispensable for mRNA stabilization during cellular stress. Nucleic Acids Res. 43, E26.

Bolger, A.M., Lohse, M., and Usadel, B. (2014). Trimmomatic : a flexible trimmer for Illumina sequence data. Bioinformatics 30, 2114–2120.

Brachmann, C.B., Davies, A., Cost, G.J., and Caputo, E. (1998). Designer Deletion Strains derived from Saccharomyces cerevisiae S288C: a useful set of strains and plasmids for PCR-mediated gene disruption and other applications. 132, 115–132.

Brengues, M., and Parker, R. (2007). Accumulation of polyadenylated mRNA, Pab1p, eIF4E, and eIF4G with P-bodies in Saccharomyces cerevisiae. 18, 2592–2602.

Buchan, J.R., and Parker, R. (2009). Eukaryotic stress granules: the ins and outs of translation. Mol. Cell 36, 932–941.

Buchan, J.R., Yoon, J., and Parker, R. (2011). Stress-specific composition, assembly and kinetics of stress granules in Saccharomyces cerevisiae. J. Cell Sci. 124, 228–239.

Buchan, J.R., Kolaitis, R., Taylor, J.P., and Parker, R. (2013). Eukaryotic stress granules are cleared by granulophagy and Cdc48 / VCP function. Cell 153, 1461–1474.

Calvo, S.E., Klauser, C.R., and Mootha, V.K. (2015). MitoCarta2.0: an updated inventory of mammalian mitochondrial proteins. Nucleic Acids Res. 44, D1251–D1257.

Chartron, J.W., Hunt, K.C.L., and Frydman, J. (2016). Cotranslational signal-independent SRP preloading during membrane targeting. Nature 536, 224–228.

Dewey, C.M., Cenik, B., Sephton, C.F., Johnson, B.A., Herz, J., and Yu, G. (2012). TDP-43 aggregation in neurodegeneration: are stress granules the key? Brain Res. 1462, 16–25.

Figley, M.D., Bieri, G., Kolaitis, R., Taylor, J.P., and Gitler, A.D. (2014). Profilin 1 associates with stress granules and ALS-linked mutations alter stress granule dynamics. J. Neuorosci. 34, 8083–8097.

Gaspar, I., Wippich, F., and Ephrussi, A. (2017). Enzymatic production of single-molecule FISH and RNA capture probes. RNA 23, 1582–1591.

Jain, S., Wheeler, J.R., Walters, R.W., Agrawal, A., Barsic, A., and Parker, R. (2016). ATPase-modulated stress granules contain a diverse proteome and substructure. Cell 164, 487–498.

Kedersha, N., and Anderson, P. (2002). Stress granules: sites of mRNA triage that regulate mRNA stability and translatability. Biochem. Soc. Trans. 30, 963–969.

Kedersha, N., Ivanov, P., and Anderson, P. (2013). Stress granules and cell signaling: more than just a passing phase? Trends Biochem. Sci. 38, 494–506.

Kedersha, N.L., Gupta, M., Li, W., Miller, I., and Anderson, P. (1999). RNA-binding proteins TIA-1 and TIAR link the phosphorylation of eIF-2a to the assembly of mammalian stress granules. J. Cell Biol. 147, 1431–1441.

Kedersha, N., Cho, M.R., Li, W., Yacono, P.W., Chen, S., Gilks, N., Golan, D.E., and Anderson, P. (2000). Dynamic shuttling of TIA-1 accompanies the recruitment of mRNA to mammalian stress granules. J. Cell Biol. 151, 1257–1268.

Kedersha, N., Chen, S., Gilks, N., Li, W., Miller, I.J., Stahl, J., and Anderson, P. (2002). Evidence that ternary complex (eIF2-GTP-tRNA iMet)–deficient preinitiation complexes are core constituents of mammalian stress granules. Mol. Biol. Cell 13, 195–210.

Kedersha, N., Panas, M.D., Achorn, C.A., Lyons, S., Tisdale, S., Hickman, T., Thomas, M., Lieberman, J., McInerney, G.M., Ivanov, P., and Anderson, P. (2016). G3BP-Caprin1-USP10 complexes mediate stress granule condensation and associate with 40S subunits. J. Cell Biol. 212, 845–860.

Kim, W.J., Kim, J.H., and Jang, S.K. (2007). Anti-inflammatory lipid mediator 15d-PGJ2 inhibits translation through inactivation of eIF4A. EMBO J. 26, 5020–5032.

Kim, D., Pertea, G., Trapnell, C., Pimentel, H., Kelley, R., and Salzberg, S.L. (2013a). TopHat2: accurate alignment of transcriptomes in the presence of insertions, deletions and gene fusions. Genome Biol. 14, 1–13.

Kim, N.C., Tresse, E., Kolaitis, R.M., Molliex, A., Thomas, R.E., Alami, N.H., Wang, B., Joshi, A., Smith, R.B., Ritson, G.P., et al. (2013b). VCP is essential for mitochondrial quality control by PINK1/Parkin and this function is impaired by VCP mutations. Neuron 78, 65–80.

Kinsella, R.J., Ka, A., Spudich, G., Almeida-king, J., Staines, D., Derwent, P., Kerhornou, A., Kersey, P., and Flicek, P. (2011). Ensembl BioMarts: a hub for data retrieval across taxonomic space. Database (Oxford) *2011*, 1–9.

Langmead, B., and Salzberg, S.L. (2012). Fast gapped-read alignment with Bowtie 2. Nat. Methods *9*, 357–360.

Langmead, B., Trapnell, C., Pop, M., and Salzberg, S.L. (2009). Ultrafast and memory-efficient alignment of short DNA sequences to the human genome. Genome Biol. *10*, R25.

Lee, S., Kopp, F., Chang, T.C., Sataluri, A., Chen, B., Sivakumar, S., Yu, H., Xie, Y., and Mendell, J.T. (2016). Noncoding RNA NORAD regulates genomic stability by sequestering PUMILIO proteins. Cell *164*, 69–80.

Li, Y.R., King, O.D., Shorter, J., and Gitler, A.D. (2013). Stress granules as crucibles of ALS pathogenesis. J. Cell Biol. *201*, 361–372.

Mackenzie, I.R., Nicholson, A.M., Sarkar, M., Boylan, K.B., Taylor, J.P., and Rademakers, R. (2017). TIA1 mutations in amyotrophic lateral sclerosis and frontotemporal dementia promote phase separation and alter stress granule dynamics. Neuron *95*, 808–816.

McEwen, E., Kedersha, N., Song, B., Scheuner, D., Gilks, N., Han, A., Chen, J.-J., Anderson, P., and Kaufman, R.J. (2005). Heme-regulated inhibitor kinase-mediated phosphorylation of eukaryotic translation initiation factor 2 inhibits translation, induces stress granule formation, and mediates survival upon arsenite exposure. J. Biol. Chem. *280*, 16925–16933.

Nagalakshmi, U., Wang, Z., Waern, K., Shou, C., Raha, D., Gerstein, M., and Snyder, M. (2008). The transcriptional landscape of the yeast genome defined by RNA sequencing. Science *320*, 1344–1349.

Nelles, D.A., Fang, M.Y., O'Connell, M.R., Xu, J.L., Markmiller, S.J., Doudna, J.A., and Yeo, G.W. (2016). Programmable RNA tracking in live cells with CRISPR/Cas9. Cell *165*, 488–496.

Neph, S., Kuehn, M.S., Reynolds, A.P., Haugen, E., Thurman, R.E., Johnson, A.K., Rynes, E., Maurano, M.T., Vierstra, J., Thomas, S., et al. (2012). BEDOPS: high-performance genomic feature operations. Bioinformatics *28*, 1919–1920.

Neymotin, B., Athanasiadou, R., and Gresham, D. (2014). Determination of in vivo RNA kinetics using RATE-seq. RNA *20*, 1645–1652.

Pagliarini, D.J., Calvo, S.E., Chang, B., Sheth, S.A., Vafai, S.B., Ong, S.E., Walford, G.A., Sugiana, C., Boneh, A., Chen, W.K., et al. (2008). A mitochondrial protein compendium elucidates complex I disease biology. Cell *134*, 112–123.

Panas, M.D., Ivanov, P., and Anderson, P. (2016). Mechanistic insights into mammalian stress granule dynamics. J. Cell Biol. *215*, 313–323.

Presnyak, V., Alhusaini, N., Chen, Y., Martin, S., Kline, N., Olson, S., Weinberg, D., Baker, K.E., Brenton, R., and Coller, J. (2016). Codon optimality is a major determinant of mRNA stability. Cell *160*, 1111–1124.

Protter, D.S.W., and Parker, R. (2016). Principles and properties of stress granules. Trends Cell Biol. *26*, 668–679.

Quinlan, A.R., and Hall, I.M. (2010). BEDTools: a flexible suite of utilities for comparing genomic features. Bioinformatics *26*, 841–842.

Radhakrishnan, A., and Green, R. (2016). Connections underlying translation and mRNA stability. J. Mol. Biol. *428*, 3558–3564.

Ramaswami, M., Taylor, J.P., and Parker, R. (2013). Altered ribostasis: RNA-protein granules in degenerative disorders. Cell *154*, 727–736.

Schwanhäussser, B., Busse, D., Li, N., Dittmar, G., Schuchhardt, J., Wolf, J., Chen, W., and Selbach, M. (2011). Global quantification of mammalian gene expression control. Nature *473*, 337–342.

Sidrauski, C., Mcgeachy, A.M., Ingolia, N.T., and Walter, P. (2015). The small molecule ISRIB reverses the effects of eIF2 α phosphorylation on translation and stress granule assembly. eLife *4*, 1–16.

Siwiak, M., and Zielenkiewicz, P. (2010). A comprehensive, quantitative, and genome-wide model of translation. PLoS Comput. Biol. *6*, e1000865.

Stoecklin, G., Stubbs, T., Kedersha, N., Wax, S., Rigby, W.F.C., Blackwell, T.K., and Anderson, P. (2004). MK2-induced tristetraprolin:14-3-3 complexes prevent stress granule association and ARE-mRNA decay. EMBO J. *23*, 1313–1324.

Stöhr, N., Lederer, M., Reinke, C., Meyer, S., Hatzfeld, M., Singer, R.H., and Hüttelmaier, S. (2006). ZBP1 regulates mRNA stability during cellular stress. J. Cell Biol. *175*, 527–534.

Tani, H., Mizutani, R., Salam, K.A., Tano, K., Ijiri, K., Wakamatsu, A., Isogai, T., Suzuki, Y., and Akimitsu, N. (2012). Genome-wide determination of RNA stability reveals hundreds of short-lived noncoding transcripts in mammals. Genome Res. *22*, 947–956.

Tichon, A., Gil, N., Lubelsky, Y., Havkin Solomon, T., Lemze, D., Itzkovitz, S., Stern-Ginossar, N., and Ulitsky, I. (2016). A conserved abundant cytoplasmic long noncoding RNA modulates repression by Pumilio proteins in human cells. Nat. Commun. *7*, 12209.

Trapnell, C., Hendrickson, D.G., Sauvageau, M., Goff, L., Rinn, J.L., and Pachter, L. (2013). Differential analysis of gene regulation at transcript resolution with RNA-seq. Nat. Biotechnol. *31*, 46–53.

Uhlen, M., Oksvold, P., Fagerberg, L., Lundberg, E., Jonasson, K., Forsberg, M., Zwahlen, M., Kampf, C., Wester, K., Hober, S., et al. (2010). Towards a knowledge-based Human Protein Atlas. Nat. Biotechnol. *28*, 1248–1250.

Uhlén, M., Fagerberg, L., Hallström, B.M., Lindskog, C., Oksvold, P., Mardinoglu, A., Sivertsson, Å., Kampf, C., Sjöstedt, E., Asplund, A., et al. (2015). Proteomics. Tissue-based map of the human proteome. Science *347*, 1260419.

Unsworth, H., Raguz, S., Edwards, H.J., Higgins, C.F., and Yagüe, E. (2010). mRNA escape from stress granule sequestration is dictated by localization to the endoplasmic reticulum. FASEB J. *24*, 3370–3380.

Van Nostrand, E.L., Pratt, G.A., Shishkin, A.A., Gelboin-Burkhart, C., Fang, M.Y., Sundararaman, B., Blue, S.M., Nguyen, T.B., Surka, C., Elkins, K., et al. (2016). Robust transcriptome-wide discovery of RNA-binding protein binding sites with enhanced CLIP (eCLIP). Nat. Methods *13*, 508–514.

Wheeler, J.R., Matheny, T., Jain, S., Abrisch, R., and Parker, R. (2016). Distinct stages in stress granule assembly and disassembly. eLife *5*, 1–25.

Xu, Z., Wei, W., Gagneur, J., Perocchi, F., Clauder-mu, S., Camblong, J., Huber, W., Steinmetz, L.M., and Guffanti, E. (2009). Bidirectional promoters generate pervasive transcription in yeast. Nature *457*, 1033–1037.

STAR★METHODS

KEY RESOURCES TABLE

REAGENT or RESOURCE	SOURCE	IDENTIFIER
Antibodies		
mouse anti-G3BP	Abcam	ab56574
rabbit anti-PABP	Abcam	ab21060
rabbit anti-PUM2	Abcam	ab10361
goat anti-mouse FITC antibody	Abcam	ab6785
donkey ant-rabbit Alexa Fluor 555 conjugate antibody	Abcam	ab150062
rabbit anti-GFP	Life Technologies	A1112
Chemicals, Peptides, and Recombinant Proteins		
Sodium (meta)arsenite	Sigma-Aldrich	S7400
RNasin Plus RNase Inhibitor	Promega	N2615
Complete mini EDTA-free protease Inhibitor	Sigma-Aldrich	11836170001
Protein A Dynabeads	Thermo Fisher Scientific	10002D
Trizol LS reagent	Thermo Fisher Scientific	10296-028
InSolution Thapsigargin – CAS	Sigma-Aldrich	586006-2mg
ddUTP-Atto633		Ephrussi lab
D-sorbitol minimum 98%	Sigma-Aldrich	S1876-1kg
Sodium azide	Sigma-Aldrich	S2002-500g
Critical Commercial Assays		
Ribo-Zero rRNA removal kit	Illumina	MRZH11124
RNA ScreenTape	Agilent	5067-5579
NEBNext Ultra Directional RNA Library Prep Kit for Illumina	New England Biolabs	E7420S
BioScientific NEXTflex Rapid Illumina Directional RNA-Seq Library Prep Kit	Bio Scientific	NOVA-5138-07
DNA-free DNA Removal Kit	Thermo Fisher Scientific	AM1906
Deposited Data		
Raw and processed sequencing files	This study	GEO: GSE99304
Experimental Models: Cell Lines		
U-2 OS G3BP1-GFP cells	Figley et al., 2014	Paul Taylor Lab
U-2 OS cells	Kedersha et al., 2016	Paul Anderson Lab
U-2 OS ΔΔG3BP1/2 cells	Kedersha et al., 2016	Paul Anderson Lab
Experimental Models: Organisms/Strains		
BY4742	Brachmann et al., 1998	Dharmacon, YSC1049
Oligonucleotides		
Stellaris FISH Probes Quasar 570 Dye TFRC	Biosearch Technologies	SMF-2006-1
Stellaris FISH Probes Quasar 570 Dye POLR2A	Biosearch Technologies	SMF-2003-1
Stellaris FISH Probes Quasar 570 Dye GAPDH	Biosearch Technologies	SMF-2026-1
Stellaris FISH Probes Quasar 670 Dye GAPDH	Biosearch Technologies	SMF-3140-1
Custom Stellaris FISH Probes (MDN1, AHNAK, DYNC1H1, PEG3, ZNF704, and NORAD)	Biosearch Technologies	Data S5
Cy3-Oligo(dT)	IDT	N/A
CDK6 20mer oligos	IDT	Data S5
Recombinant DNA		
pRP1363 (Pab1-GFP, Ura3)	Brengues and Parker, 2007	N/A

(Continued on next page)

Continued

REAGENT or RESOURCE	SOURCE	IDENTIFIER
Software and Algorithms		
Trimmomatic 0.32	Bolger et al., 2014	http://www.usadellab.org/cms/?page= trimmomatic
Bowtie 0.12.7	Langmead et al., 2009	http://bowtie-bio.sourceforge.net/ index.shtml
HTSeq	Anders et al., 2015	https://htseq.readthedocs.io/en/release_0.9.1/
DESeq 1.22.1	Anders and Huber, 2010	http://bioconductor.org/packages/release/ bioc/html/DESeq.html
Bowtie2 2.0.2	Langmead and Salzberg, 2012	http://bowtie-bio.sourceforge.net/bowtie2/ index.shtml
Tophat 2.0.6	Kim et al., 2013b	http://ccb.jhu.edu/software/tophat/index. shtml
Cuffdiff 2.2.1	Trapnell et al., 2013	http://cole-trapnell-lab.github.io/cufflinks/ cuffdiff/
MATLAB R2016b	MathWorks	https://www.mathworks.com/products/ matlab.html
R Studio 0.99.491	Rstudio	https://www.rstudio.com/
Imaris Image Analysis Software 8.4.1	Bitplane	http://www.bitplane.com/
Prism 7 for Mac OS X	Graphpad	https://www.graphpad.com

U-2 OS GROWTH CONDITIONS AND REAGENTS

Human osteosarcoma U-2 OS cells expressing G3BP1-GFP (Figley et al., 2014), U-2 OS cells and U-2 OS ΔΔG3BP1/2 cells (Keder-sha et al., 2016), maintained in DMEM with high glucose, 10% fetal bovine serum, and 1% penicillin/streptomycin at 37°C/5% CO_2, were used in all experiments.

ISOLATION OF RNA FROM U-2 OS CELLS AND SG CORES FOR RNA-SEQUENCING

U-2 OS cells expressing G3BP1-GFP were grown to 85% confluency in three 500 cm^2 square TC-treated culture dishes (Thermo Fisher Scientific, 07-200-599). One hour prior to stress, cell culture media was exchanged with fresh media. Cells were then treated with 500 μM $NaAsO_2$ for 1 hr at 37°C/5% CO_2. After stress, cells were washed once with media, transferred to falcon tubes, and pelleted at 1,500 x g for 3 min. Upon aspirating the media, the pellets were immediately flash-frozen in liquid N_2 and stored at −80°C until isolation of mammalian SG cores was performed.

The isolation of SG cores was adapted from two papers (Jain et al., 2016; Wheeler et al., 2016). Briefly, the pellet was thawed on ice for 5 min, re-suspended in 1 mL SG lysis buffer (50 mM TrisHCl pH 7.4, 100 mM KOAc, 2 mM MgOAc, 0.5 mM DTT, 50 μg/mL Heparin, 0.5% NP40, complete mini EDTA-free protease inhibitor (Sigma Aldrich, 11836170001), 1 U/μL of RNasin Plus RNase Inhibitor (Promega, N2615) and passed through a 25 gauge 5/8 needle attached to a 1 mL syringe 7 times. After lysis, the lysates were spun at 1000 x g for 5 min at 4°C to pellet cell debris. 50 μL and 950 μL of the supernatants were transferred to new microcentrifuge tubes for isolating total and SG RNAs respectively (Figure S1A). For isolating total RNA, Trizol LS reagent (Thermo Fisher Scientific, 10296-028) was added and RNA was extracted following the manufacturers protocol. Following isopropanol precipitation, the RNA pellet was re-suspended in 50 μL RNase-free H_2O.

The following steps were performed to isolate mammalian SG cores and extract its RNA: 1) The 950 μL supernatant was spun at 18,000 x g for 20 min at 4°C to pellet SG cores. 2) The resulting supernatant was discarded, and the pellet was re-suspended in 1 mL SG lysis buffer. 3) Steps 1 and 2 were repeated to enrich for SG cores. 4) The resulting pellet was then re-suspended in 300 μL of SG lysis buffer and spun at 850 x g for 2 min at 4°C. 5) The supernatant which represents the mammalian SG core enriched fraction was transferred to a new tube. 6) The enriched fraction was pre-cleared twice by adding 60 μL equilibrated DEPC-treated Protein A Dynabeads (Thermo Fisher Scientific, 10002D) and nutating at 4°C for 30 min. Dynabeads were removed using a magnet. 7) 20 μL of anti-GFP antibody (Life technologies, A1112) was added to the enriched fraction and nutated at 4°C for 1 hr to affinity purify SG cores. 8) The solution was spun at 18,000 x g for 20 min at 4°C and the supernatant was discarded to remove any unbound antibody. 9) The pellet was then re-suspended in 500 μL SG lysis buffer and 60 μL equilibrated DEPC-treated Protein A Dynabeads. 10) The sample was nutated for 3 hr at 4°C. 11) The Dynabeads were washed three times with wash buffer 1 (20 mM Tris HCl pH 8.0, 200 mM NaCl, 1 U/μL of RNasin Plus RNase Inhibitor) for 5 min, once with wash buffer 2 (20 mM Tris HCl pH 8.0, 500 mM NaCl, 1 U/μL of RNasin Plus RNase Inhibitor) for 5 min, and once with wash buffer 3 (SG lysis buffer + 2M Urea, 1 U/μL of RNasin Plus RNase

Inhibitor) for 2 min at 4°C. 12) The beads were resuspended in 200 μL of 100 μg/mL Protease K solution (1X TE buffer, 2M Urea, 1 U/μL of RNasin Plus RNase Inhibitor) and incubated for 15 min at 37°C. 13) Trizol LS reagent (Thermo Fisher Scientific, 10296-028) was added to the samples and RNA was extracted following the manufacturers protocol. Following isopropanol precipitation, the RNA pellet was re-suspended in 20 μL RNase-free H_2O.

MAMMALIAN LIBRARY CONSTRUCTION AND RNA-SEQUENCING

After isolating RNA from cells and SG cores 1 and 20 μL of RNA isolated from cells and SG cores, respectively, were treated with rDNase 1 following manufacturer's protocol (Thermo Fisher Scientific, AM1906). Immediately, the samples were ribosomal-depleted using Ribo-Zero rRNA removal kit following manufacturer's protocol (Illumina, MRZH11124). Afterward, the quality of the RNA was inspected using high sensitivity RNA ScreenTape (Agilent, 5067-5579) on Agilent TapeStation 2200 instrument (University of Colorado-Boulder BioFrontiers Next-Generation Sequencing Facility).

cDNA libraries were prepared following manufacturer's protocol from three replicates of 10 ng ribosomal-depleted RNA from cells and SG cores using NEBNext Ultra Directional RNA Library Prep Kit for Illumina (New England Biolabs, E7420S). The qualities and amounts of the cDNA libraries were assessed using high sensitivity D1000 ScreenTape (Agilent, 5067-5584) on Agilent Tapestation 2200 instrument and the Qubit (Thermo Fisher Scientific), respectively (University of Colorado-Boulder BioFrontiers Next-Generation Sequencing Facility) The cDNA libraries (3 from cells and 3 from SG cores) were pooled and sequenced on the Illumina NextSeq 500 platform using the High Output 150 cycles kit (paired-end reads, single index) (University of Colorado-Boulder BioFrontiers Next-Generation Sequencing Facility).

ISOLATION AND SEQUENCING OF RNA FROM STRESS GRANULES

A 2.4L culture of Pab1-GFP expressing yeast cells and stressed them with sodium azide (NaN_3) for 30', prior to lysis. Total cellular RNA ($Total_{RNA}$) and RNA from stress granule cores (SG_{RNA}) were isolated from this culture as described in a previous report (Jain et al., 2016).

YEAST LIBRARY CONSTRUCTION

Libraries were constructed using the Bio Scientific NEXTflex Rapid Illumina Directional RNA-Seq Library Prep Kit. We followed the manufacturer supplied directions. Before making the library, the RNA was ribosome depleted using the Ribo-Zero rRNA removal kit, also according to manufacturer's directions. The resulting RNA was incubated with Turbo DNase at 37°C for 1 hr and then cleaned up using a Zymo Research RNA Clean and Concentrator kit also according to the manufacturer's directions.

YEAST SEQUENCING DATA ANALYSIS

Read quality was assessed using fastqc. Illumina adapters were trimmed using Trimmomatic 0.32 in single end (SE) mode (Bolger et al., 2014). An index genome was built with Bowtie 0.12.7 using the 'build' command and the S288C reference genome version (R64-1-1), which was acquired through *Saccharomyces* Genome Database (SGD)(Langmead et al., 2009). Reads were aligned using Bowtie 0.12.7 using the following options: -S -v 2 -m 3 –best. Reads mapping to each gene were counted using HTSeq with parameters –t gene –l Name –f sam –s reverse, using the R64-1-1 annotation file (Anders et al., 2015). Normalization and differential expression analysis were then performed using DESeq 1.22.1 (Anders and Huber, 2010).

SUTs and CUTs were analyzed using the same method, but with a different annotation file gene annotation file that contained these transcript annotations (Xu et al., 2009).

YEAST LENGTH, TRANSLATION, AND STABILITY ANALYSIS

Length: Data for the length analysis was obtained from a previous report (Nagalakshmi et al., 2008). *Codon Optimality:* The fraction of the optimal codon for each gene was calculated using a custom script based on codon stabilization coefficients presented in a previous report (Presnyak et al., 2016). In brief, the amount of each codon was tallied on a gene by gene basis. Optimal codons were assigned a value of one while non-optimal codons were assigned a value of zero. The total number of optimal codons was then divided by the total number of codons in order to find the fraction of optimal codons. Predicted translation initiation rates and ribosome density data were obtained from a previous study (Siwiak and Zielenkiewicz, 2010) *Stability:* RNA half-lives were obtained from a previous report (Neymotin et al., 2014). All boxplots were generated using PRISM. Scatterplots were created using PRISM and Tableau.

MAMMALIAN SEQUENCING DATA ANALYSIS

Read quality was assessed using fastqc. Illumina adaptors were trimmed using Trimmomatic 0.32 in paired and (PE) mode (Bolger et al., 2014). An index genome was acquired from GENCODE (Release 19 GRCh37.p13). Reads were aligned using Tophat (version 2.0.6) and Bowtie2 (version 2.0.2) and the following parameters:–b2 –fast –microexon-search (Kim et al., 2013a; Langmead and Salzberg, 2012). Differential expression analysis was performed using Cuffdiff (version 2.2.1) with the default parameters (Trapnell et al., 2013).

HUMAN LENGTH, TRANSLATION, AND STABILITY ANALYSIS

All length data (5′UTR, ORF, 3′ UTR and total) was acquired using Ensemble's Biomart tool (Aken et al., 2016; Kinsella et al., 2011). Translational efficiency values were calculated from a previous report (Ribosome protected fragment reads / RNA-seq reads) (Sidrauski et al., 2015). GC content data were acquired using Ensemble's Biomart tool. Half-life data were acquired from a previous report (Tani et al., 2012).

eCLIP DATA ANALYSIS

All eCLIP data were analyzed from a previous report, which examined eCLIP targets of over 80 proteins (Van Nostrand et al., 2016). We examined eCLIP data from known RBPs in the SG proteome as well as non-SG proteins (Jain et al., 2016). In brief, a bed file for each eCLIP experiment was obtained from the ENCODE data repository, which contained the genomic coordinates of all eCLIP peaks. Next, a bed file was created for the human genome using NCBI's gtf annotation file. The program BEDOPS v2.4.26 was used performed to convert the gtf file into a bed file, using the command 'gtf2bed' (Neph et al., 2012). The human genome bed file was then compared to each eCLIP bed file using the 'intersect' command in bedtools version 2.16.2, in order to see which genes contained eCLIP peaks (Quinlan and Hall, 2010). The fraction of eCLIP peaks in SG-enriched mRNAs was calculated for a given RBP by dividing the summation of eCLIP peaks aligning to SG-enriched mRNAs by the total number of eCLIP peaks. A similar analysis was done for SG-depleted mRNAs.

MACHINE LEARNING

A mathematical model for mRNA localization during stress was built using MATLAB's "Classification Learner" application. For yeast mRNA localization, two parameters (length and fraction optimal codons), and a response (mRNA localization) were imported into the classification learner. The model used 90% of the data for training and held back 10% for testing. This process was performed for multiple iterations until every mRNA had been used for both model building and model testing. The course nearest neighbor model provided the best results. In brief, the course nearest neighbor model makes localization predictions of a given mRNA based on the localization of its 100 nearest neighbors on a scatterplot of length versus codon optimality. A similar approach was used for modeling mammalian mRNA localization, but instead using ribosome translational efficiency of codon optimality.

STATISTICAL TESTS

R^2 values were calculated for pairwise comparison of sequencing replicates by squaring MATLAB's 'corr' function. To calculate the statistical significance in boxplots, a 2-sample t test was performed using PRISM software. A 2-population proportion test was used in R to calculate the overlap of yeast SG enriched and SG depleted mRNA with SRP-localized and mitochondria-localized mRNA.

STRESS CONDITIONS

To examine mRNA localization during other stresses, we used the following stress conditions in U-2 OS cells. Thapsigargin was added to a final concentration of 1 μM for 1 hr. For heat shock experiments, cells were placed at 42°C for 1 hr. For osmotic stress, cells were stressed in 0.4M sorbitol for 2.5 hr.

SEQUENTIAL IMMUNOFLUORESCENCE AND SINGLE MOLECULE FISH

Sequential immunofluorescence and smFISH on fixed U-2 OS and U-2 OS ΔΔG3BP1/2 cells were performed following manufacturer's protocol (https://biosearchassets.blob.core.windows.net/assets/bti_custom_stellaris_immunofluorescence_seq_protocol.pdf) in Figures 1 and 5 and Figure S1. SmFISH on fixed U-2 OS cells expressing G3BP1-GFP were performed following manufacturer's protocol (https://biosearchassets.blob.core.windows.net/assets/bti_stellaris_protocol_adherent_cell.pdf) in Figure 2 and 3. smFISH on yeast cells was performed following the manufacturer's&protocol&(https://biosearchassets.blob.core.windows.net/assets/bti_custom_stellaris_yeast_protocol.pdf).

The primary antibodies used for immunofluorescence include mouse anti-G3BP (5 µg/mL, ab56574(Abcam)), rabbit anti-PABP (1 µg/mL, ab21060(Abcam)), and/or rabbit anti-PUM2 (5 µg/mL, ab10361(Abcam)) and the appropriate secondary antibodies used were goat anti-mouse FITC antibody (1:500, Abcam (ab6785)), and donkey anti-rabbit Alexa Fluor 555 conjugate antibody (1:500, Abcam(ab150062)). Ship ready Stellaris FISH Probes recognizing TFRC, POLR2A, and GAPDH transcripts labeled with Quasar 570 Dye and GAPDH labeled with Quasar 670 Dye (SMF-2006-1, SMF-2003-1, SMF-2026-1, and SMF-3140-1, respectively, Biosearch Technologies, Petaluma, CA) and Custom Stellaris FISH Probes designed against AHNAK, DYNC1H1, PEG3, ZNF704, NORAD, and MDN1 transcripts labeled with Quasar 670 dye by utilizing the Stellaris RNA FISH Probe Designer (Biosearch Technologies, Petaluma, CA), available online at http://www.biosearchtech.com/stellaris-designer (version 4.2), were used. CDK6 mFISH probes labeled with Atto633 were designed following Gaspar et al. (2017). ddUTP-Atto633 were provided to us by Ephrussi lab, and CDK6 22-mer reverse complement DNA oligos were purchased from IDT. Finally, oligo d(T)30-Cy3 were purchased from IDT.

MICROSCOPY AND IMAGE ANALYSIS

Fixed U-2 OS, U-2 OS ΔΔG3BP1/2, U-2 OS G3BP1-GFP, and yeast cells stained by immunofluorescence, smFISH and/or DAPI were imaged using a wide field DeltaVision Elite microscope with a 100X objective using a PCO Edge sCMOS camera. At least five images were taken for each experiment comprising of 25 Z sections each in Figure 1, 2, Figure S1 and 5. This analysis allows us to capture the entire cell and provide us the means to estimate the number of transcripts in cell and SGs by best fit-line analysis in Figure 2. In Figure 3 and Figure S2, at least 10 images were taken for each experiment comprising 5 Z sections. All images shown in the manuscript are one Z-plane and image processed by ImageJ with FIJI plugin and Adobe Photoshop. Minimum and Maximum display values were set in ImageJ for each channel to properly view fluorescence. Quantification of smFISH spots in SGs in cells was determined using the spot and cell functions from Imaris Image Analysis Software (Bitplane) (University of Colorado-Boulder, BioFrontiers Advanced Light Microscopy Core).

DATA AND SOFTWARE AVAILABILITY

Raw sequencing data for both yeast and mammalian SGs and total RNA are available for download GEO: GSE99304.